Intensity Dependence of Coulomb-Repulsion Effect in Strong-Field Nonsequential Double Ionization

T.D.H. Truong[a,b,c], T.D. Anh-Tai[d], H.H. Nguyen[a], N.H. Nha[b,c], D.H. Dung[e] and V.N.T. Pham[a,f,*]

[a] *Department of Physics, Ho Chi Minh City University of Education, Ho Chi Minh City, Vietnam*
[b] *Department of Theoretical Physics, University of Science, Ho Chi Minh City 700000, Vietnam*
[c] *Vietnam National University, Ho Chi Minh City 700000, Vietnam*
[d] *Quantum Systems Unit, Okinawa Institute of Science and Technology Graduate University, Onna, Okinawa 904-0495, Japan*
[e] *Department of Natural Science, Dong Nai University, Dong Nai, Vietnam*
[f] *International Cooperation Office, Ho Chi Minh City University of Education, Ho Chi Minh City, Vietnam*

Received: 15.12.2021 & Accepted: 05.04.2022

Doi: 10.12693/APhysPolA.141.569 *e-mail: vinhpnt@hcmue.edu.vn

The nonsequential double ionization of the argon atom is studied in this article using an orthogonal two-color laser pulse with different intensities. The results demonstrate that electron correlation is strongly dependent on the relative phase of the laser pulses. We also observe that the recollision time remains constant when analyzing the nonsequential double ionization signal at the relative phase 0.6π. Meanwhile, the contribution of each returning bunch of the first ionized electron and the final electron–electron repulsion highly depends on the laser intensity. Coulomb repulsion is most pronounced at low and high laser intensities. However, at moderate laser intensities, it does not sufficiently affect the momentum distribution.

topics: Coulomb repulsion, orthogonal two-color laser, nonsequential double ionization process, Yukawa potential

1. Introduction

Since its discovery in 1975 [1], the nonsequential double ionization (NSDI) process has been extensively investigated as a powerful tool for studying the electron–electron (e–e) correlation toward the recollision process [2–7]. It is well established that NSDI is explicable using the simple man model [8]. In this model, when an atom/molecule is exposed to a laser field, the first electron is ionized by the combined atomic/molecular and laser potentials. The electric field accelerates the first ionized electron, which is then driven back to recollide with its parent ion when the electric field reverses, thereby initiating the ionization of the second electron. NSDI can occur toward the recollision via two widely accepted mechanisms, depending on the returning energy of the first ionized electron and how it shares this energy with the bounded one: direct recollision ionization (e, $2e$), in which the first ionized electron directly knocks out the second one after recollision [9, 10], and recollision-induced excitation with subsequent ionization (RESI), in which the second electron is excited upon recollision and then ionized by the laser field, while the first electron remains free [2] or is recaptured to form the doubly excited state [6, 11, 12].

While being driven by the laser field to trigger the NSDI process, the first ionized electron may efficiently transfer its energy to the bounded one in the first return, or it must recollide with the parent ion several times [13]. Multiple recollision can contaminate the final e–e correlation signals, such as the correlated two-electron momentum distributions (CTEMD) [14]. To demonstrate the pure manipulation of the e–e correlation with respect to the recollision process, one should alleviate multiple recollisions by increasing the laser field's intensity and/or wavelength [15]. Alternatively, the orthogonal two-color laser pulse (OTC) can be used [16]. Since its inception in 2005 [17], the OTC has gained widespread recognition for its ability to significantly control the returning time, recollision energy, and NSDI yield by varying the relative phase [16–19] or intensity [20]. Thus, OTC fields can exert control over the CTEMD (in two directions for each of the OTC's two field components) [16]. The OTC was used in particular to theoretically control the correlated dynamics in NSDI for He atoms by varying the relative phase [16], to analyze the mechanisms governing the NSDI of Xe atoms [19], to study the dependence of Ne^{2+} yields on relative phase, taking into account the change in recollision time when adjusting the laser intensity at

a particular relative phase [20], and to experimentally demonstrate, for the first time, the possibility of controlling the two-electron emission dynamics on the subcycle scale for Ne [21]. Additionally, the OTC was used to investigate the HeH^+ molecule's NSDI process, demonstrating that the correlated pattern in CTEMD is dependent on the relative phase and intensity ratio (I_2/I_1) of the two-color field [18].

Interestingly, as shown in [16, 20, 21], the temporal window of recollision moments can be controlled to locate within a very narrow range. Additionally, the results in [16, 20, 21] indicated that at some particular relative phases of the OTC, the returning bunches of the first ionized electrons are efficiently split into two distinct groups. However, no additional research on the dynamics of these returning groups has been published. The mechanisms by which the recollision time, the contribution of each returning group to the drift CTEMD, and the role of the Coulomb repulsion associated with the NDSI process change as the laser intensity varies, remain unknown and deserve thorough investigation. We also note that while the role of the final Coulomb repulsion has been revisited several times for atomic [12, 22–24] and molecular systems [25], this effect in the OTC laser field is still unavailable. Using the classical ensemble model [12, 25–27], we numerically examine the NSDI of the Ar atom induced by the OTC laser field at several representative relative phases. We then focus on the relative phase at the maximum of the Ar^{2+} yield, where the range of recollision time is shortest, in order to conduct a thorough investigation of the NSDI mechanism, Coulomb repulsion, and the dynamics of two ionized electrons as the laser intensity is varied. It is interesting to observe that the recollision time remains constant as the laser intensity is altered. Meanwhile, the contribution of each returning group and the role of Coulomb repulsion are highly dependent on the intensity of the laser.

The organization of the paper is as follows. Section 2 provides a brief overview of the classical ensemble model used to study the NSDI process in the presence of the OTC laser pulse. In Sect. 3, we present and discuss numerical results relating the Ar^{2+} yield to the relative phase of the OTC laser pulse and the e–e correlated dynamic, resulting in CTEMD behavior along the 800 nm field's polarization direction. Here, the comprehensive analysis at the relative phase $\Delta\varphi = 0.6\pi$ is performed. The paper is concluded in Sect. 4.

2. Method

In our calculation, we employ the classical three-dimensional ensemble model, which has been widely used in the framework of the NSDI process [12, 25–27] due to its significant advantages [26]. This method is described in detail in [27]. According to the classical model, the motion of two electrons is governed by the Newton equation (atomic units are used throughout this paper unless otherwise specified)

$$\frac{\mathrm{d}^2\boldsymbol{r}_i}{\mathrm{d}t^2} = -\nabla\Big[V_{ne}(\boldsymbol{r}_i) + V_{ee}(\boldsymbol{r}_1, \boldsymbol{r}_2)\Big] - \boldsymbol{E}(t), \quad (1)$$

where the subscript i is the label of the two electrons, $\boldsymbol{r}_i$ is the position of the i-th electron, and $\boldsymbol{E}(t)$ is the electric field. The electric field of the OTC has the form

$$\boldsymbol{E}(t) = E_1(t)\hat{x} + E_2(t)\hat{y}, \quad (2)$$

in which

$$E_1(t) = E_{01}\,\cos(\omega_1 t)\,f(t), \quad (3)$$

$$E_2(t) = E_{01}\,\cos\left(\omega_2 t + \Delta\varphi\right)\,f(t). \quad (4)$$

Here $f(t)$ is the trapezoidal envelope of the laser pulse including two-cycle turn-ons, six cycles at full strength, and two-cycle turn-offs, $\Delta\varphi$ is the relative phase between two components of the OTC field. It is noted that $E_1(t)$ and $E_2(t)$ are respectively linearly polarized in the x and y axes. The wavelengths of the two component fields are $\lambda_1 = 800$ nm and $\lambda_2 = 400$ nm, and their intensities are equal. Here

$$V_{ne}\left(\boldsymbol{r}_i\right) = -\frac{2}{\sqrt{\boldsymbol{r}_i^2 + a^2}}, \quad (5)$$

and

$$V_{ee}\left(\boldsymbol{r}_1, \boldsymbol{r}_2\right) = \frac{1}{\sqrt{\left(\boldsymbol{r}_1 - \boldsymbol{r}_2\right)^2 + b^2}}, \quad (6)$$

are the electron-ion attractive and the e–e repulsive potentials, respectively. To avoid autoionization of the Coulomb interaction, the soft parameters a and b are considered [9, 15, 28]. We set $a = 1.5$ a.u. and $b = 0.05$ a.u. for Ar [29–32]. The ensembles have a total size of 5 million particles.

To simulate the NSDI process, we solve (1) for each atom in the ensemble using the fourth-order Runge–Kutta method [33]. It is worth noting that in the classical model, electrons are transferred to the continuum solely through the mechanism of over-the-barrier ionization. Thus, the systems can be well characterized by ionization energy. To obtain the initial condition, the ensemble is populated from a classically allowed position for the argon ground-state energy of -1.59 a.u. The available kinetic energy is distributed randomly in the momentum space between two electrons. The electrons are then allowed to evolve for a sufficient amount of time (≈ 200 a.u.) in the absence of the laser field in order to achieve stable position clustering around the origin and a stable momentum distribution [28, 34]. It should be noted that properly chosen initial conditions enable the generation of a suitable set of classical trajectories that closely approximate the quantum momentum function [35].

The laser is turned on to initiate the NSDI process of the ensemble. At the end of the pulse, the energy of each ionized electron (including the kinetic energy, electron–ion attractive potential energy, and

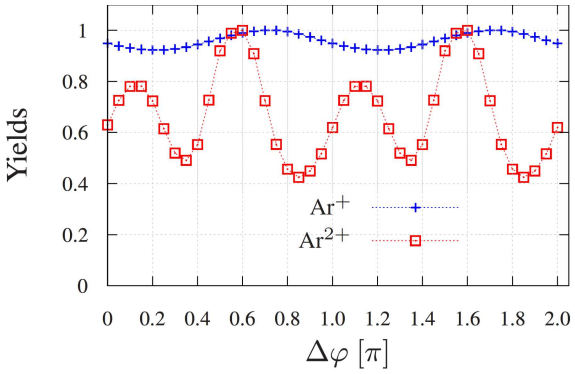

Fig. 1. The dependence of the yields of Ar^+ and Ar^{2+} ions on the relative phase $\Delta\varphi$ of the OTC laser field for the laser intensity $I = 1.5 \times 10^{14}$ W/cm^2.

half of the repulsive e–e potential energy) in each atom is analyzed. Only when both electrons have positive energy is the atom considered to be double ionized (DI) [25, 28, 34].

To investigate the role of the e–e repulsive Coulomb interaction in the NSDI process, we performed an additional calculation, in which the final state e–e repulsion at the DI moment is neglected and replaced by the Yukawa potential as

$$V'_{ee}(\boldsymbol{r}_1, \boldsymbol{r}_2) = \frac{\exp\left(-\lambda\sqrt{(\boldsymbol{r}_1 - \boldsymbol{r}_2)^2 + b^2}\right)}{\sqrt{\left(\boldsymbol{r}_1 - \boldsymbol{r}_2\right)^2 + b^2}}, \quad (7)$$

with the screening parameter $\lambda = 5$ [22, 28], which is sufficiently large to rapidly truncate the interaction between two electrons just after they escape from the parent ion [28, 34].

3. Results

We proceed to discuss the NSDI process of Ar induced by OTC laser pulses, the parameters of which are listed in Sect. 2. The yields of Ar^+ and Ar^{2+} ions as functions of relative phase $\Delta\varphi$ for the laser intensity $I = 1.5 \times 10^{14}$ W/cm^2 are shown in Fig. 1. The results are presented only for the relative phase in the interval $0 \leq \Delta\varphi \leq 2\pi$ due to the periodicity of the laser pulse. Take note that the yields have been normalized such that the maximum values equal unity.

The Ar^+ signal oscillates slightly and approaches saturation since it is directly related to the atom's ionization rate, which is mainly dependent on the laser intensity and atomic ionization potential [36]. Meanwhile, the Ar^{2+} yield exhibits a strong dependence on $\Delta\varphi$, with maxima occurring around $\Delta\varphi = (0.1 + \frac{n}{2})\pi$, and minima located around $\Delta\varphi = (0.35 + \frac{n}{2})\pi$, where $n \in \mathbb{N}$. We also note that the signals of Ar^{2+} are primarily associated with the NSDI process at the laser intensity used in our calculation. At higher intensities, the sequential double ionization (SDI) process becomes more pronounced.

Although there is no experimental evidence for this structure in the case of Ar, we believe our result is reliable because a similar trend has been observed experimentally [21] and studied theoretically [20] for Ne^{2+}. According to [21], the recollision probability is greatest at relative phases with the smallest initial transverse velocity and vice versa [37], because effective recollision induced by OTC fields requires an appropriate initial transverse velocity at the first ionization [17].

A detailed understanding of the dynamics of two-electron emission can be gained by examining the CTEMD. The CTEMDs along the 800 nm field direction are shown in Fig. 2 for four representative values of the relative phases $\Delta\varphi$ that correspond to two components of the OTC fields in phase ($\Delta\varphi = 0\pi$ — Fig. 2a); the signal of Ar^{2+} ion being minimal ($\Delta\varphi = 0.35\pi$ — Fig. 2b, $\Delta\varphi = 0.85\pi$ — Fig. 2d) and maximal ($\Delta\varphi = 0.6\pi$ — Fig. 2c). The laser intensity used in this investigation is $I = 1.5 \times 10^{14}$ W/cm^2.

When the relative phase is $\Delta\varphi = 0$, the CTEMD is clustered in the first and third quadrants and exhibits symmetry about the main diagonal. Here, most of the two ionized electrons escape to similar hemispheres with equivalent momenta. When the relative phase is increased to $\Delta\varphi = 0.35\pi$, the CTEMD expands to four quadrants, with the strongest signals observed in the third quadrant, indicating that the two ionized electrons exhibit both correlated and anticorrelated behaviors. The interesting pattern is observed at the relative phase $\Delta\varphi = 0.6\pi$, where the CTEMD splits into two distinct groups, i.e., the first group located primarily in the third quadrant, and the second one divided into two sets along the p_{1x} and p_{2x} axes. Here, the two electrons are either ionized in the same hemisphere with comparable momenta or in opposite directions with significantly different momenta. For $\Delta\varphi = 0.85\pi$, the CTEMD is mainly concentrated in the third quadrant, but also includes the first quadrant. These results demonstrate that the correlation between two ionized electrons can be controlled by adjusting the relative phase of the OTC pulses, as concluded in [16].

To gain a better understanding of the $\Delta\varphi$-dependence of CTEMD, we perform a back trajectory analysis [16, 20] on the NSDI trajectories associated with the CTEMDs in Fig. 2a–d versus the laser phase at the instant of recollision, as shown in Figs. 2e-2h, respectively. Note that the recollision moment is defined as the instant when the distance between the first ionized electron and its parent ion approaches a minimum [28]. The solid blue and dashed green curves depict the electric fields of the 800 nm and 400 nm pulses, respectively, within an optical cycle. The drift momentum of an ionized electron at time t_i induced by an oscillatory field $E = E_0 \cos(\omega t)$ is composed of two terms: the initial velocity (v_0) and the velocity gained from the vector potential, as $\left(\left(-\frac{E_0}{\omega}\right)\sin(\omega t_i)\right)$ [16].

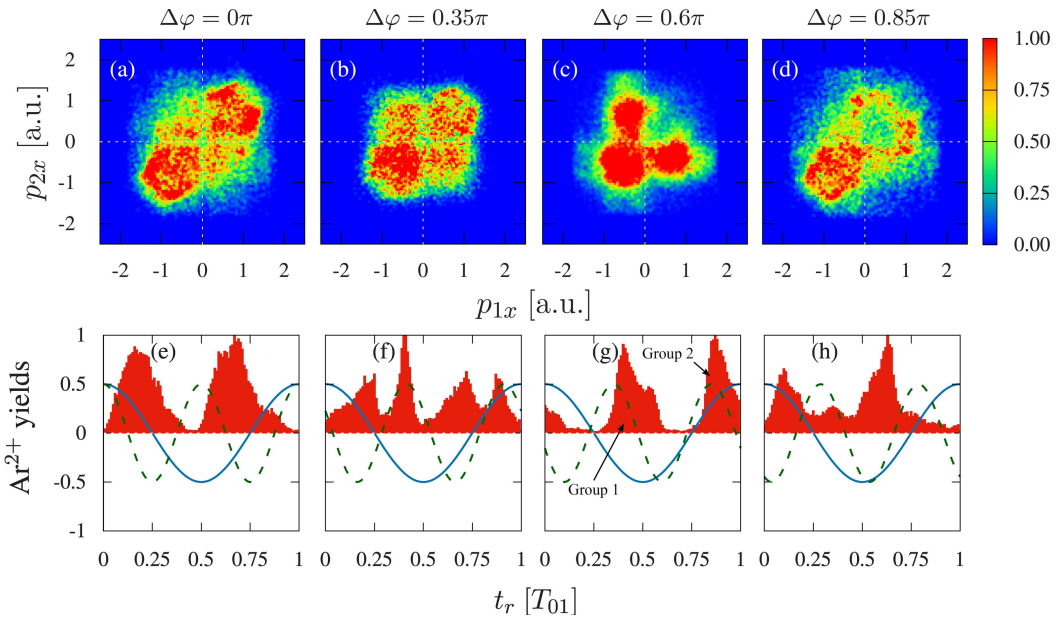

Fig. 2. (a)–(d) CTEMDs along the polarization axis of the 800 nm field of the OTC pulse and (e)–(h) counts of NSDI trajectories versus laser phase at the instant of recollision for the laser intensity $I = 1.5 \times 10^{14}$ W/cm^2 at four representative relative phases phases $\Delta\varphi = 0\pi, 0.35\pi, 0.6\pi, 0.85\pi$, respectively. The solid blue and dashed green curves illustrate the electric fields associated with the 800 nm and 400 nm pulses, respectively, and $T_{01} = \frac{2\pi}{\omega_1}$ is the period of the 800 nm field.

In the case of $\Delta\varphi = 0$ (Fig. 2e), there are two distinct clusters of recollision electrons, and the majority of recollisions occur near the zero crossings of the 800 nm electric field. The first electron flies out of the atom around $0.1T_{01}$ after recolliding. The second electron is then ionized at a time difference around $0.15T_{01}$. Moreover, at the instant of ionization, the initial velocities of two electrons are close to zero [16]. As a result, they are ionized sequentially during the same quarter-cycle of the laser field, producing the correlated pattern shown in Fig. 2a. Recollisions eventually leading to NSDI occur over a wide range for $\Delta\varphi = 0.35\pi$ (Fig. 2f) and $\Delta\varphi = 0.85\pi$ (Fig. 2h). Thus, two terms in the final velocity of two electrons are competitive, and the CTEMDs are distributed across four quadrants, as illustrated in Fig. 2b and d. For $\Delta\varphi = 0.6\pi$, there are two distinct bunches of recollision electrons at the trough and peak of the 800 nm laser field. Unlike the case for $\Delta\varphi = 0$, the contributions of two recollision bunches result in the formation of two distinct patterns in the CTEMD, including a group of correlated signals in the third quadrant and two groups along the p_{1x} and p_{2x} axes (see Fig. 2c). Additionally, our investigation indicates that at this relative phase, the electrons returning to the core near the field's extremum have lower recolliding energies. This fact is well consistent with the simple man model [8]. As a result, the recollision electrons do not gain enough energy to directly ionize the bounded electron toward recollision. However, in this case, the electric field significantly suppresses the atomic potential at the instant of recollision, allowing one of the two electrons to escape from the atom over-the-barrier immediately after recollision, while the other electron ionizes at the subsequent peaks. This mechanism is responsible for the generation of correlated signals in CTEMD. In some instances, both electrons may be ionized simultaneously after recollision. The e–e repulsion is significant and can considerately accelerate one electron while blocking the other, resulting in a significant difference in the drift momenta of two ionized electrons [25].

We focus on systematically analyzing the mechanisms of NSDI and the role of the e–e repulsion associated with each bunch of recollision electrons for the specific relative phase $\Delta\varphi = 0.6\pi$. Figure 3 demonstrates that the CTEMD originated from the trajectories of recollision group 1 (see Fig. 2g). The signal converges primarily to the third quadrant in this case (Fig. 3d), indicating a side-by-side DI in which the two ionized electrons escape the parent ion with equivalent velocity parallel to the direction of the electric field. The delay time (t_{DI}) between the recollision and double ionization moments has the most prominent peak around $0.5T_{01}$ and extends to $4T_{01}$, with peaks separating by T_{01} (Fig. 3a). Additionally, the difference between the ionization instants (Δt) of two electrons after recollision significantly focuses at $0.25T_{01}$ (Fig. 3b). As illustrated in Fig. 3c, the energy-sharing energy of two electrons after the recollision moment is symmetric. This result shows that the dominant mechanism of double ionization is RESI. After the moment of recollision, one of the two electrons

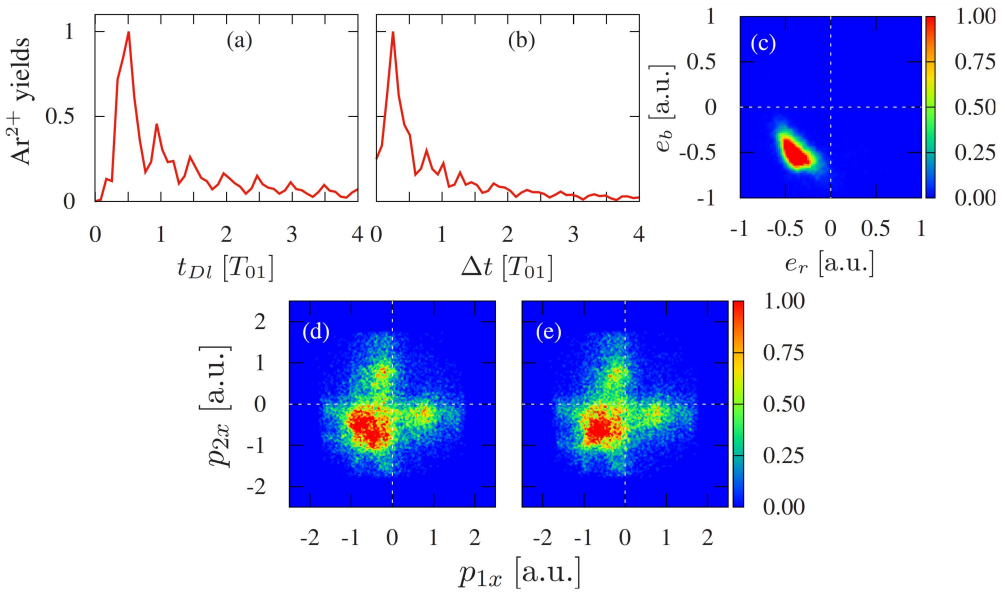

Fig. 3. (a) The delay time between DI and recollision moments, (b) the difference between the ionization instants of two electrons after recollision, (c) the energy of recolliding and bounded electrons after recollision, (d) the CTEMD associating with the recollision group 1 in Fig. 2g, and (e) the same CTEMD when neglecting the final state electron–electron repulsion by replacing the Yukawa potential. The results are investigated for the recollision group 1 at $\Delta\varphi = 0.6\pi$ and laser intensity $I = 1.5 \times 10^{14}$ W/cm^2.

ionizes from the atom via the over-the-barrier ionization mechanism. The other electron then moves into the excited state and escapes from the ion core in a similar quarter cycle of the electric field. As a result, their drift momenta are comparable, as observed in Fig. 3d. To investigate the role of final e–e repulsion, we apply the Yukawa potential immediately after the instant of double ionization in order to bypass the Coulomb explosion between two ionized electrons. The result is shown in Fig. 3e. The CTEMD with Yukawa potential is nearly identical to that in Fig. 3d, demonstrating that Coulomb repulsion plays no role in the CTMED associating with recollision group 1 for laser intensity $I = 1.5 \times 10^{14}$ W/cm^2 at $\Delta\varphi = 0.6\pi$. It is worth noting that the CTEMDs distribution in Fig. 3d and e changes slightly when some DI events converge on the main diagonal of Fig. 3e. This is explained by the fact that DI cases exhibit near-simultaneous ionization of two electrons in Fig. 3b, indicating that the final e–e repulsion contributes to the CTEMD spectrum. According to our calculations, these DI events account for approximately 7.93%.

Figure 4a depicts the extracting result from CTEMD in Fig. 2c for recollision group 2 at $\Delta\varphi = 0.6\pi$ for $I = 1.5 \times 10^{14}$ W/cm^2. The signals are concentrated mostly along two axes, with a small portion in the third quadrant along the primary diagonal. According to Fig. 4b, the delay time is especially concentrated in the range of $0.15T_{01}$ to $0.25T_{01}$ and slightly extends to $4T_{01}$. To investigate the microscopic mechanisms governing the NSDI process of Ar atom, we classify double ionization events according to their delay time, which is less than or greater than $0.25T_{01}$, corresponding to the direct ionization (e-2e) or RESI mechanisms, respectively [9, 10]. Figure 4c–f and Fig. 4g–j illustrate the analysis for these two scenarios, respectively. When $t_{\rm DI} < 0.25T_{01}$, the momentum spectrum focuses in the second and fourth quadrants along the secondary diagonal (Fig. 4e), implying that the two electrons ionize with similar magnitudes but opposite directions of momenta. Our results demonstrate that the symmetric energy sharing between two electrons toward the recollision process exists (see Fig. 4d), and that two electrons almost simultaneously escape from the parent ion (see Fig. 4c). These characteristics support the (e–2e) mechanism. In Fig. 4f, we show the CTEMD without regard for the final state Coulomb repulsion. As can be seen, portions of the signals tend to shrink to the origin, while the rest remains unchanged. Thus, the Coulomb explosion is critical only at the beginning of double ionization and for pairs of electrons that gain small drift moments due to being ionized nearly simultaneously and traveling at small velocities. The Coulomb interactions between two ionized electrons dissipate rapidly as high-velocity electrons depart from each other. A similar analysis for $t_{\rm DI} > 0.25T_{01}$ demonstrates that the Coulomb repulsion has no effect on the formation of the CTEMD, as the spectra in Fig. 4i and j, corresponding to the absence and application of the Yukawa potential, are nearly identical. Indeed, in this case, there is a highly asymmetric energy sharing process toward recollision (see Fig. 4h). Thus, one electron retains the necessary energy to ionize first,

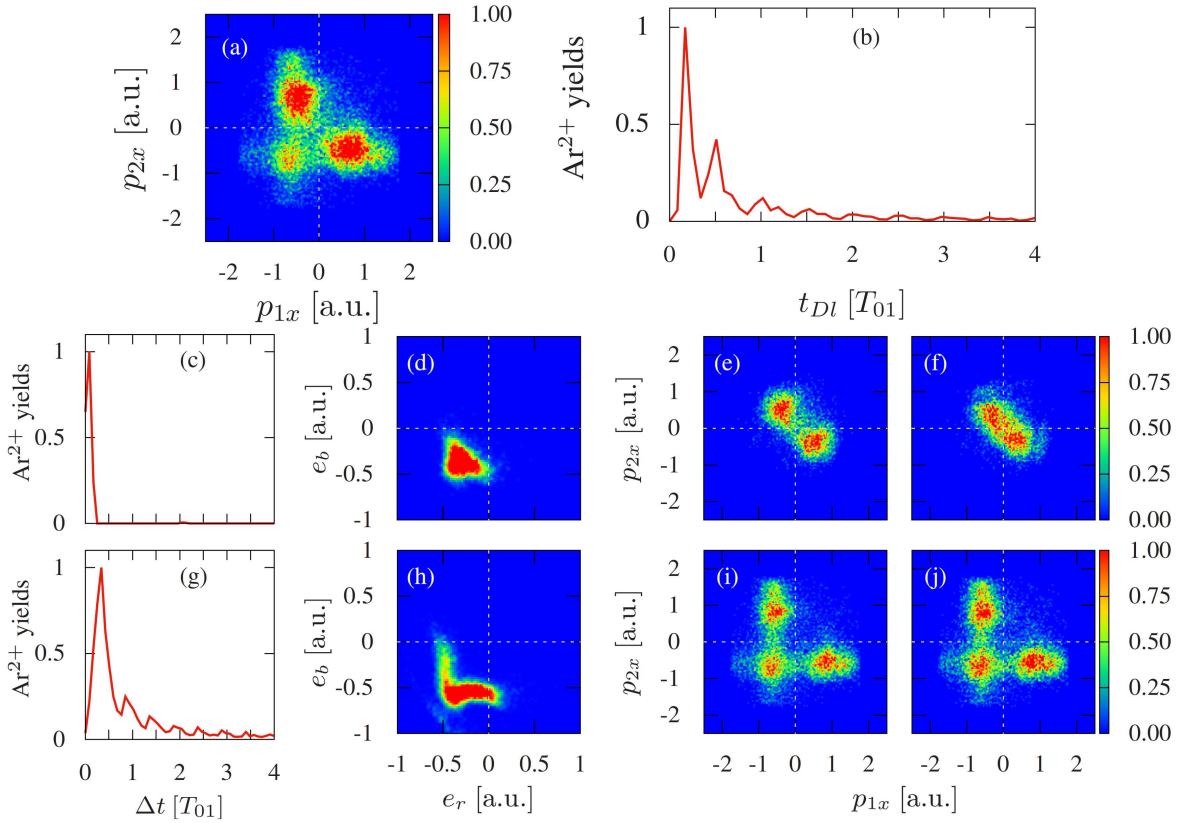

Fig. 4. (a) The CTEMD associated with the recollision group 2 in Fig. 2g, (b) the delay time between DI and recollision moments; (c)–(f) the difference between the ionization instants of two electrons after recollision time, the energy of recolliding and bounded electrons after recollision, the CTEMD with and without applying the Yukawa potential for $t_{\rm DI} < 0.25T_{01}$; (g)–(j) similar to (c)–(f) but for $t_{\rm DI} > 0.25T_{01}$. The results are investigated for the recollision group 2 at $\Delta\varphi = 0.6\pi$ for the laser intensity $I = 1.5 \times 10^{14}$ W/cm^2.

while the second electron transfers a small amount of recollision energy to jump to an excitation state and then escapes from the parent ion after a time difference that mostly peaks around $0.5T_{01}$ (see Fig. 2g). This is referred to as the RESI mechanism.

Next, we examine the mechanisms of NSDI and the role of the e–e repulsion associated with each bunch of recollision for specific relative phase at laser intensities ranging from $I = 1.0\times10^{14}$ W/cm^2 to $I = 2.0\times10^{14}$ W/cm^2, which are below and above the recollision-ionization threshold, respectively. It is worth noting that in the classical model, after ionizing the neutral atom Ar, the recollision-ionization threshold is equal to the energy required to ionize the ion Ar^+ to Ar^{2+}, thereby causing double ionization. The laser intensity is said to be saturated when the maximum returning energy of the recolliding electron induced by the laser field equals the recollision-ionization threshold.

Figure 5 shows the CTEMD and NSDI trajectories versus the laser phase at the instant of recollision for $I = 1.0 \times 10^{14}$ W/cm^2 (Fig. 5a, b) and $I = 2.0 \times 10^{14}$ W/cm^2 (Fig. 5e, f). It is obvious that the recollision instants remain constant as the laser intensity changes. There are asymmetric contributions to the CTEMD from two bunches of recollision electrons of $I = 1.0 \times 10^{14}$ W/cm^2 and $I = 2.0 \times 10^{14}$ W/cm^2, with the dominance associated with group 2 (Fig. 5b) and group 1 (Fig. 5f), respectively. Meanwhile, in the case of $I = 1.5 \times 10^{14}$ W/cm^2 (Fig. 2g), two recollision bunches provide equivalent contributions. The signals in CTEMDs are divided into two parts corresponding to two recollision bunches, as illustrated in Fig. 5c and g for group 1 and Fig. 5d and h for group 2, for $I = 1.0 \times 10^{14}$ W/cm^2 (panels c and d) and $I = 2.0 \times 10^{14}$ W/cm^2 (panels g and h), respectively. For the low intensity, the momentum spectrum of group 1 produces an arc-like structure from the second to the fourth quadrants (Fig. 5c). It then shifts to the third quadrant for saturation intensity (Fig. 3d) and finally to the negative axes for high intensity (Fig. 5g). However, in the case of group 2, the momentum distribution is concentrated on the positive axes at low intensity (Fig. 5d), then translates to the second and fourth quadrants (Fig. 4a) at moderate intensity, and finally forms an arc-like structure at a high intensity (Fig. 5h). Figure 5 reflects the contribution of each recollision group and demonstrates the critical role of these recollision groups in forming the final CTEMD.

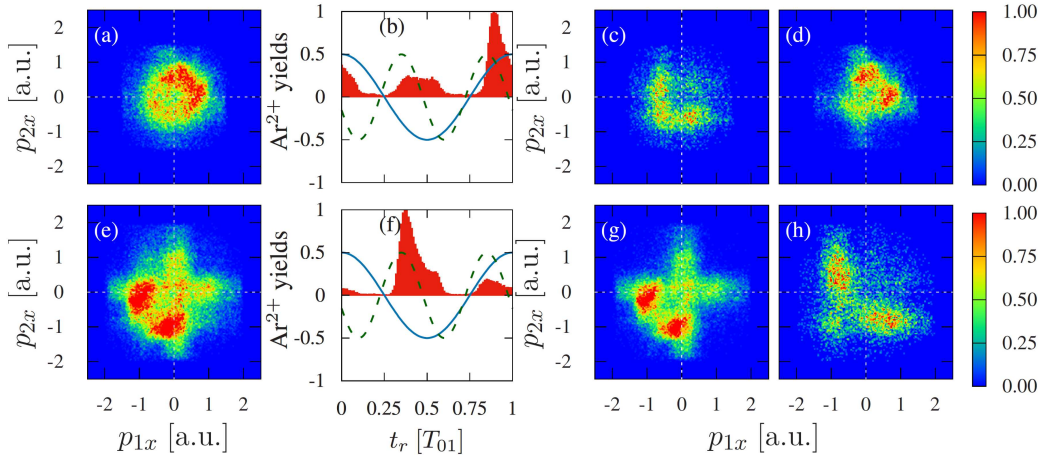

Fig. 5. (a)–(d) The CTEMD along the polarization axis of the 800 nm field of the OTC pulse, the counts of NSDI trajectories versus the laser phase at the instant of recollision, the CTEMDs associated with recollision groups 1 and 2 at the relative phase $\Delta\varphi = 0.6\pi$ for the laser intensity $I = 1.0 \times 10^{14}$ W/cm^2; (e)–(h) similar to (a)–(d) but for laser intensity $I = 2.0 \times 10^{14}$ W/cm^2. The solid blue and dashed green curves represent the electric fields associated with the 800 nm and 400 nm pulses, respectively, and T_{01} is the period of the 800 nm field.

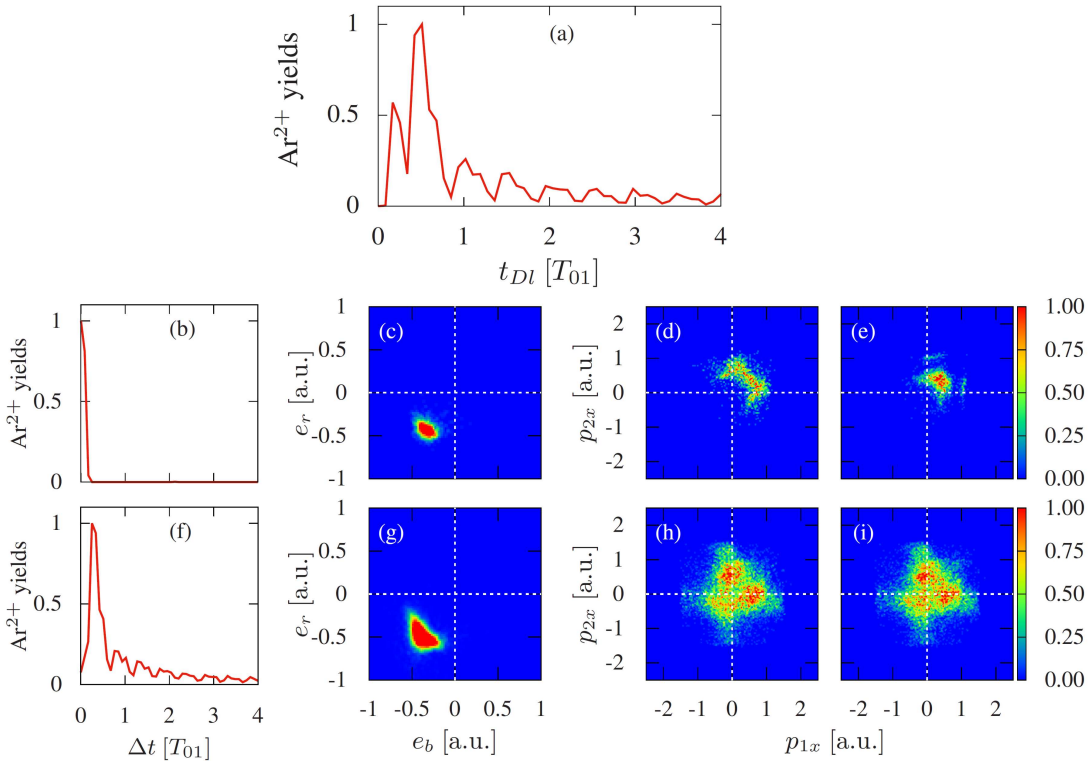

Fig. 6. (a) The delay time between DI and recollision moments; (b)–(e) the difference between the ionization instants of two electrons after recollision time, the energy of recolliding and bounded electrons after recollision, the CTEMD with and without applying the Yukawa potential for $t_{\rm DI} < 0.25T_{01}$; (f)–(i) similar to (b)–(e) but for $t_{\rm DI} > 0.25T_{01}$. The results are investigated for the recollision group 2 at $\Delta\varphi = 0.6\pi$ for the laser intensity $I = 1.0 \times 10^{14}$ W/cm^2.

In the case of $I = 1.0 \times 10^{14}$ W/cm^2 at $\Delta\varphi = 0.6\pi$, recollision group 2 contributes more to the final CTEMD than group 1. Thus, we concentrate on the dynamics of two ionized electrons in group 2, as illustrated in Fig. 6. According to Fig. 6a, the majority of DI events occur prior to T_{01} from the recollision moment, with a peak around $0.5T_{01}$. Two electrons ionize almost simultaneously in the direct ionization mechanism associated with $t_{\rm DI} < 0.25T_{01}$ (Fig. 6b), and the sharing energy is

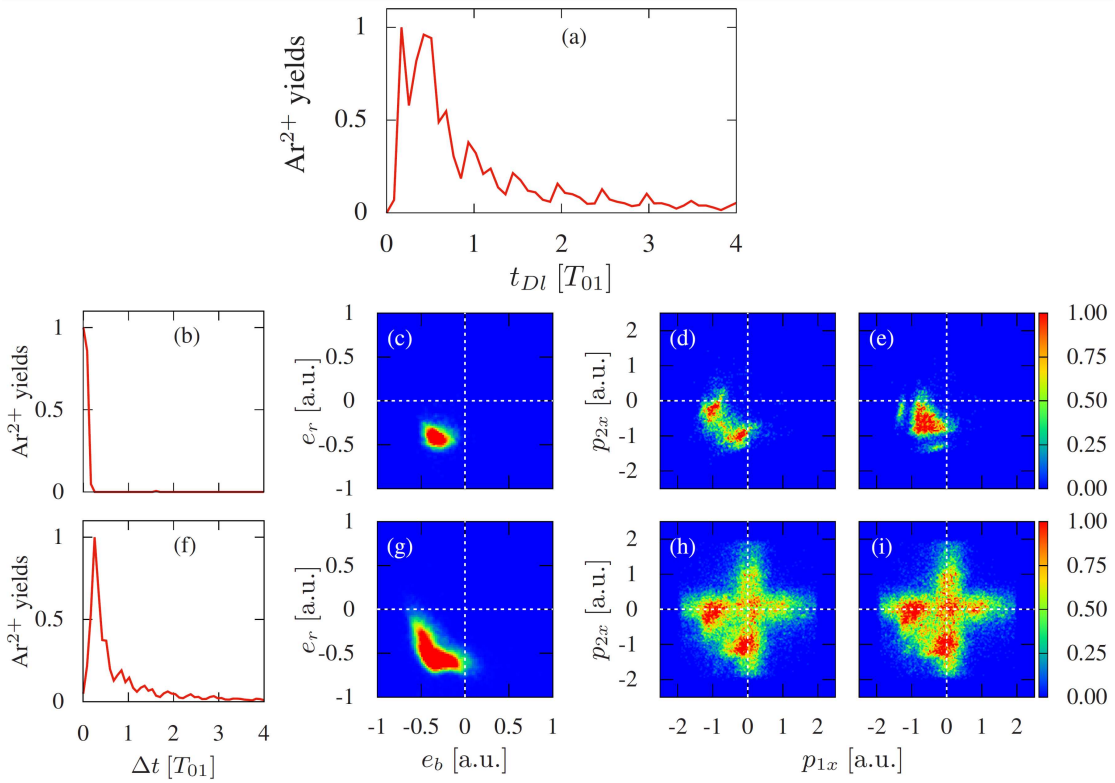

Fig. 7. Similar to Fig. 6 but for the recollision group 1 at $\Delta\varphi = 0.6\pi$ for the laser intensity $I = 2.0 \times 10^{14}$ W/cm^2.

highly symmetric (Fig. 6c). As illustrated in Fig. 6d, the CTEMD signals appear along a line segment in the first quadrant, implying that two ionized electrons leave the parent ion in the same direction but with different drift momenta. By accelerating one electron and decelerating the other, the final e–e repulsion has a significant effect on the final CTEMD. By applying the Yukawa potential to screen off the Coulomb interaction, the signals are clearly shrunk to the primary diagonal, as observed in Fig. 6e. Meanwhile, when the NSDI occurs via the RESI mechanism, the final e–e repulsion plays a minor role. The results for $t_{\rm DI} > 0.25T_{01}$ (Fig. 6f–i) are similar to those previously discussed for $I = 1.5 \times 10^{14}$ W/cm^2.

Finally, we investigate the role of the final e-e repulsion at $\Delta\varphi = 0.6\pi$ for the high laser intensity of $I = 2.0 \times 10^{14}$ W/cm^2. Here, we focus on the dominant recollision group 1's behavior and present the results in Fig. 7. The majority of DI events are widely expanded in the range of $T_{Dl} < T_{01}$ (Fig. 7a). For the (e–2e) mechanism with $t_{\rm DI} < 0.25T_{01}$, two electrons are ionized nearly simultaneously (Fig. 7b), share energy symmetrically toward the recollision process (Fig. 7c), and fly to the same direction, which is opposite to the 800 nm electric field. Thus, when the Yukawa potential is used instead of the e–e Coulomb repulsive one, the CTEMD evolves from the line segment (Fig. 7d) to the primary diagonal (Fig. 7e) in the third quadrant. This feature confirms the importance of the final e–e Coulomb repulsion in this instance. Again, the results for $t_{\rm DI} > 0.25T_{01}$, $I = 2.0 \times 10^{14}$ W/cm^2 (Fig. 7f–i) are similar to those obtained for $I = 1.0 \times 10^{14}$ W/cm^2 and $I = 1.5 \times 10^{14}$ W/cm^2.

4. Conclusions

To summarize, we investigated the attosecond dynamics of the NSDI process induced by OTC laser pulses. Correlations between two electrons are highly dependent on the relative phase of the OTC pulses. We then focus our attention on the role of Coulomb repulsion and two electron dynamics at relative phase $\Delta\varphi = 0.6\pi$ for the low ($I = 1.0 \times 10^{14}$ W/cm^2), moderate ($I = 1.5 \times 10^{14}$ W/cm^2), and high ($I = 2.0 \times 10^{14}$ W/cm^2) laser intensities. Intriguingly, the returning electrons are separated into two distinct bunches with a narrow range of recollision time. The moment of recollision between two returning bunches remains constant as the laser intensity varies, but the contribution of each bunch varies. It's also worth noting that the energy shared between two electrons upon recollision, as well as the role of the final Coulomb repulsion associated with each returning bunch, is highly dependent on the laser intensity. By combining the relative phase and intensity of the OTC pulse, we can sufficiently control the dynamic of recollision on a subcycle scale.

Acknowledgments

This work was supported by the Ho Chi Minh City University of Education, Vietnam, under grant number CS.2020.19.50. The authors wish to express their gratitude to Prof. Yueming Zhou of Huazhong University of Science and Technology for his insightful advice. Tran Duong Anh-Tai gratefully thanks for the support provided by Okinawa Institute of Science and Technology Graduate University (OIST), including the Scientific Computing & Data Analysis Section at OIST.

References

[1] V. Suran, I. Zapesochnyi, *Sov. Tech. Phys. Lett.* **1**, 2 (1975).

[2] B. Feuerstein, R. Moshammer, D. Fischer et al., *Phys. Rev. Lett.* **87**, 043003 (2001).

[3] A. Rudenko, V.L.B. de Jesus, T. Ergler, K. Zrost, B. Feuerstein, C.D. Schröter, R. Moshammer, J. Ullrich, *Phys. Rev. Lett.* **99**, 263003 (2007).

[4] B. Bergues, M. Kübel, N.G. Johnson et al., *Nat. Commun.* **3**, 813 (2012).

[5] C. Zhangjin, A. Zhou, T. Morishita, Y. Bai, X. Hao, O. Zatsarinny, K. Bartschat, *Phys. Rev. A* **103**, 053102 (2021).

[6] X. Hao, Y. Bai, C. Li, J. Zhang, W. Li, W. Yang, M. Liu, J. Chen, *Commun. Phys.* **5**, 31 (2022).

[7] F. Sun, X. Chen, W. Zhang et al., *Phys. Rev. A* **101**, 021402 (2020).

[8] P.B. Corkum, *Phys. Rev. Lett.* **71**, 1994 (1993).

[9] Y.-B. Li, X. Wang, Q.-B. Tang, G.-H. Wang, J.-G. Man, *Sci. Rep* **6**, 37413 (2016).

[10] T.-T. Xu, J.-H. Chen, X.-F. Pan, H.-D. Zhang, S. Ben, X.-S. Liu, *Chin. Phys. B* **27**, 093201 (2018).

[11] B. Eckhardt, J.S. Prauzner-Bechcicki, K. Sacha, J. Zakrzewski, *Chem. Phys.* **370**, 168 (2010).

[12] Y. Zhou, C. Huang, P. Lu, *Phys. Rev. A* **84**, 023405 (2011).

[13] Y. Liu, S. Tschuch, A. Rudenko, M. Dürr, M. Siegel, U. Morgner, R. Moshammer, J. Ullrich, *Phys. Rev. Lett.* **101**, 053001 (2008).

[14] P.J. Ho, J.H. Eberly, *Phys. Rev. Lett.* **95**, 193002 (2005).

[15] X. Ma, Y. Zhou, P. Lu, *Phys. Rev. A* **93**, 013425 (2016).

[16] Y. Zhou, C. Huang, A. Tong, Q. Liao, P. Lu, *Opt. Exp.* **19**, 2301 (2011).

[17] M. Kitzler, M. Lezius, *Phys. Rev. Lett.* **95**, 253001 (2005).

[18] A. Tong, Y. Deng, G. Feng, *Opt. Commun.* **285**, 2368 (2012).

[19] L. Chen, Y. Zhou, C. Huang, Q. Zhang, P. Lu, *Phys. Rev. A* **88**, 043425 (2013).

[20] Z. Yuan, D. Ye, Q. Xia, J. Liu, L. Fu, *Phys. Rev. A* **91**, 063417 (2015).

[21] L. Zhang, X. Xie, S. Roither et al., *Phys. Rev. Lett.* **112**, 193002 (2014).

[22] D.F. Ye, X. Liu, J. Liu, *Phys. Rev. Lett.* **101**, 233003 (2008).

[23] Z. Chen, Y. Liang, C.D. Lin, *Phys. Rev. Lett.* **104**, 253201 (2010).

[24] N. Camus, B. Fischer, M. Kremer et al., *Phys. Rev. Lett.* **108**, 073003 (2012).

[25] C. Huang, W. Guo, Y. Zhou, Z. Wu, *Phys. Rev. A* **93**, 013416 (2016).

[26] S.L. Haan, L. Breen, A. Karim, J.H. Eberly, *Phys. Rev. Lett.* **97**, 103008 (2006).

[27] S.L. Haan, L. Breen, A. Karim, J.H. Eberly, *Opt. Exp.* **15**, 767 (2007).

[28] Y. Zhou, L. Qing, P. Lu, *Phys. Rev. A* **82**, 053402 (2010).

[29] B. Yu, Y. Li, *J. Mod. Opt.* **59**, 1797 (2012).

[30] J.-H. Chen, T.-T. Xu, T. Han, Y. Sun, Q.-Y. Xu, X.-S. Liu, *Chin. Phys. B* **29**, 013203 (2020).

[31] C. Huang, M. Zhong, Z. Wu, *Opt. Exp.* **27**, 7616 (2019).

[32] J.-H. Chen, Q. Zhen, X.-S. Liu, *Opt. Commun.* **499**, 127263 (2021).

[33] H.P. William, A. Teukolsky, W.T. Vetterling, B.P. Flannery, *Numerical Recipes in Fortran*, Cambridge University Press, Cambridge 1992.

[34] T.D.H. Truong, T.V.N. Hao, V.N.T. Pham, *J. Phys.: Conf. Ser.* **1274**, 012007 (2019).

[35] S. Hack, S. Majorosi, M.G. Benedict, S. Varró, A. Czirják, *Phys. Rev. A* **104**, 031102 (2021).

[36] M.V. Ammosov, N.B. Delone, V.P. Krainov, *Sov. Phys. JETP* **64**, 1191 (1986).

[37] N.B. Delone, V.P. Krainov, *J. Opt. Soc. Am. B* **8**, 1207 (1991).